Title

Facet-specific interaction between methanol and TiO2 probed by sum-frequency vibrational spectroscopy

Journal

Proceedings of the National Academy of Sciences of the United States of America, 115(17)

ISSN

0027-8424

Authors

Yang, Deheng
Li, Yadong
Liu, Xinyi
et al.

Publication Date

2018-04-24

DOI

10.1073/pnas.1802741115

Peer reviewed

Facet-specific interaction between methanol and TiO_2 probed by sum-frequency vibrational spectroscopy

Deheng Yang[a,b], Yadong Li[c], Xinyi Liu[a,b], Yue Cao[a,b], Yi Gao[c,1], Y. Ron Shen[a,b,d,1], and Wei-Tao Liu[a,b,e,1]

[a]State Key Laboratory of Surface Physics, Physics Department, Fudan University, Shanghai 200433, China; [b]Key Laboratory of Micro and Nano Photonic Structures, Fudan University, Shanghai 200433, China; [c]Division of Interfacial Water, Key Laboratory of Interfacial Physics and Technology, Shanghai Institute of Applied Physics, Chinese Academy of Sciences, 201800 Shanghai, China; [d]Department of Physics, University of California, Berkeley, CA 94720; and [e]Collaborative Innovation Center of Advanced Microstructures, Nanjing 210093, China

Contributed by Y. Ron Shen, March 21, 2018 (sent for review February 14, 2018; reviewed by Mary Jane Shultz and Xueming Yang)

The facet-specific interaction between molecules and crystalline catalysts, such as titanium dioxides (TiO_2), has attracted much attention due to possible facet-dependent reactivity. Using surface-sensitive sum-frequency vibrational spectroscopy, we have studied how methanol interacts with different common facets of crystalline TiO_2, including rutile(110), (001), (100), and anatase(101), under ambient temperature and pressure. We found that methanol adsorbs predominantly in the molecular form on all of the four surfaces, while spontaneous dissociation into methoxy occurs preferentially when these surfaces become defective. Extraction of Fermi resonance coupling between stretch and bending modes of the methyl group in analyzing adsorbed methanol spectra allows determination of the methanol adsorption isotherm. The isotherms obtained for the four surfaces are nearly the same, yielding two adsorbed Gibbs free energies associated with two different adsorption configurations singled out by ab initio calculations. They are (*i*) ∼−20 kJ/mol for methanol with its oxygen attached to a low-coordinated surface titanium, and (*ii*) ∼−5 kJ/mol for methanol hydrogen-bonded to a surface oxygen and a neighboring methanol molecule. Despite similar adsorption energetics, the Fermi resonance coupling strength for adsorbed methanol appears to depend sensitively on the surface facet and coverage.

titanium dioxide | facet effect | adsorption configuration | sum-frequency vibration spectroscopy | Fermi resonance

Catalytic activity of a crystal may depend sensitively on its facet. Thus, recent studies on heterogeneous catalysis on nanocrystals, including metals, alloys, and oxides, have focused on controlling their facets to optimize selectivity and efficiency of catalytic reactions (1–3). It however requires detailed knowledge about molecular adsorption and reaction on each single facet, and such knowledge under ambient temperature and atmosphere is still hardly available. This is the case for many oxides. Titanium dioxide (TiO_2) is among the most important photocatalysts due to its abundance, nontoxicity, high reactivity, and chemical stability (4–7). It is also a benchmark model system for investigating photocatalysis such as water splitting, alcohol dissociation (8), and more recently, reduction of CO_2 (3). In fact, research on facet engineering of oxide catalysts has been mostly carried out on TiO_2 (1–3). Over the years, substantial progress has been made in comprehending molecular interactions with different surfaces of TiO_2 through both theoretical and experimental means, but a wide gap still exists between the two. Calculations are usually on adsorption energetics of molecules on well-defined, (nearly) stoichiometric single-crystal surfaces (9–13), while experiments on catalytic reactions are often on nanocrystals with a number of different facets (1–3). To seek consensus with theories and search for understanding of how reactivity depends on surface crystalline structures, experimental investigation on individual single crystal surfaces is obviously essential. Temperature-programmed desorption (TPD) (14–19) and scanning tunneling microscopy (STM) (20–24) have been employed in the past for such studies. The former can yield adsorption energetics of molecules on a surface; unfortunately, it generally cannot detect as-adsorbed species and their adsorption configurations. The latter can monitor surface morphology and energy levels, but has difficulty in identifying chemical species and their binding configurations. Moreover, these techniques are usually operable only in ultrahigh vacuum (UHV), and not applicable to samples in real environment.

Surface-specific sum-frequency vibrational spectroscopy (SFVS) has been proven to be an effective tool for probing molecular adsorption on surfaces in real atmosphere (25–27). It can selectively detect adsorbates, provide information on their adsorption configurations and bonding geometries, and work under a wide range of pressure and temperature, allowing deduction of adsorption isotherms and energetics of adsorbates on surfaces to directly compare with theory (28–30). The technique has been applied to probe adsorption of small molecules, including methanol, on TiO_2 (31–40). However, a comprehensive study of molecular adsorption on different facets of TiO_2, in correlation with theory, has not yet been reported.

In this article, we report an SFVS study of methanol adsorption on four different TiO_2 surfaces: rutile(110), (100), (001), and anatase(101), which are the commonly investigated facets of TiO_2. Methanol is of particular interest because it not only is a prototype model reactant, but also has numerous technological applications (8). The SFVS experiment was conducted with samples at room temperature and under a wide range of methanol

Significance

Facet engineering has become a major strategy for designing crystalline catalysts, yet many fundamental issues, including facet-specific interaction with adsorbates, remain unsolved due to lack of experimental investigation. Using surface-specific sum-frequency vibrational spectroscopy, we have conducted an in-depth study of methanol adsorption on four different facets of TiO_2 under ambient conditions. The spectra revealed that for the four facets investigated, dissociation of adsorbed methanol occurs only when surface defects are present. Adsorption kinetics and energetics appeared nearly the same on different facets, but the Fermi resonance coupling strength for CH_3 of adsorbed methanol was found to depend sensitively on facets and methanol coverage, and could serve as a gauge for studying facet effects on molecular adsorption and surface reactions.

Author contributions: Y.R.S. and W.-T.L. designed research; D.Y., Y.L., X.L., Y.C., and Y.G. performed research; D.Y., Y.G., and W.-T.L. analyzed and interpreted data; and Y.G., Y.R.S., and W.-T.L. wrote the paper.

Reviewers: M.J.S., Tufts University; and X.Y., Dalian Institute of Chemical Physics.

The authors declare no conflict of interest.

[1]To whom correspondence may be addressed. Email: gaoyi@sinap.ac.cn, yrshen@berkeley.edu, or wtliu@fudan.edu.cn.

This article contains supporting information online at www.pnas.org/lookup/suppl/doi:10.1073/pnas.1802741115/-/DCSupplemental.

Published online April 9, 2018.

vapor pressures, with results corroborated by ab initio calculations. They provide detailed understanding of how methanol molecules interact with different surfaces. Whether methanol adsorbs on TiO_2 in the molecular form or dissociates spontaneously has long been a controversial topic. By monitoring the SF vibrational spectra in the CH stretching region, we found unambiguously that on all four surfaces of TiO_2 under ambient conditions, methanol only appeared in the undissociated molecular form; dissociation into methoxy was only observed in the presence of surface defects. In analyzing the SF vibrational spectra, we discovered the Fermi resonance (FR) coupling, which mixes the nearly degenerate CH_3 symmetric stretching mode (r^+) and bending overtone (2δ) of methanol, was sensitive to the TiO_2 surface structure as well as methanol coverage on the surface. With the FR coupling effect separated, the adsorption isotherm of methanol on a surface could then be obtained from the amplitude of the CH_3-r^+ mode versus methanol vapor pressure. For all of the four surfaces of TiO_2, fitting the isotherms by the Langmuir model led to the conclusion that there were two adsorption configurations with adsorption free energies of ~ -20 kJ/mol and ~ -5 kJ/mol, respectively. Our ab initio calculation showed that the former corresponded to methanol bonded to a surface Ti atom, and the latter to methanol hydrogen-bonded to a surface oxygen atom as well as a neighboring adsorbed methanol. According to the calculation, sensitivity of the FR coupling to TiO_2 surfaces seems to be correlated with the hydrogen bonding (H-bonding) strength of the adsorbed methanol molecules. As it is suggested that H bonds have strong and profound effects on TiO_2 surface reactions (41), the significantly longer H-bonding length of methanol on anatase(101) than on rutile(110) may contribute to the usually observed higher reactivity on anatase, in particular, anatase nanoparticles.

Results and Discussion

The basic theory of SFVS is described in detail elsewhere (25, 42). Briefly, when the IR frequency is near a surface vibrational resonance, the SF signal is proportional to $|\overleftrightarrow{\chi}_{NR} + \overleftrightarrow{\chi}_R|^2$, where $\overleftrightarrow{\chi}_{NR}$ is the nonresonant background, and

$$\overleftrightarrow{\chi}_R = \sum_q \frac{\overleftrightarrow{A}_q}{\omega_{IR} - \omega_q + i\Gamma_q} \quad [1]$$

is the resonant contribution, with $\overleftrightarrow{A}_q$, ω_q, and Γ_q being the amplitude, frequency, and damping coefficient of the qth resonance mode, respectively. Fig. 1 shows the SSP (referring to S-polarized SF output, S-polarized near-IR input, and P-polarized IR input, respectively) spectra in the 2,800–3,000-cm^{-1} range from the four TiO_2 crystal surfaces under various methanol vapor pressures. All spectra exhibit sharp resonance peaks from the adsorbed methanol, and a nonresonant background from TiO_2, which was minimized by adjusting the azimuthal orientation of the crystal surface as in previous studies (43) (*SI Appendix*, Fig. S1).

We focus here on the methanol CH stretching modes. All spectra in Fig. 1 can be fitted using Eq. **1** with two dominant peaks (an example is shown in the Fig. 1*A*, *Inset*), centered at ~2,860 and 2,965 cm^{-1} for low methanol vapor pressure, and red-shifted to about 2,840 and 2,950 cm^{-1} for saturation vapor pressure (P_s). The lower and higher frequency modes are known to be the CH_3-r^+ and FR modes of methanol, respectively (44, 45), but the latter originates from the overtone (2δ) of the bending mode and both modes are affected by FR coupling. Supposedly, there is another, weaker FR mode arising from coupling between the CH_3-r^+ and bending overtone at ~2,920 cm^{-1} (46–48), but it is too weak to be observed here by SFVS with the SSP polarization combination.

Fig. 2 (solid symbols) presents the SSP amplitudes, A_{r+} and A_{FR}, for the methanol CH_3-r^+ and FR modes, respectively, versus the partial pressure of methanol, $p_r = P/P_s$. Since both modes are from the methyl group, we would expect A_{r+} and A_{FR} to have the same pressure dependence, and with A_{r+} and A_{FR} proportional to the surface density of methanol, their pressure

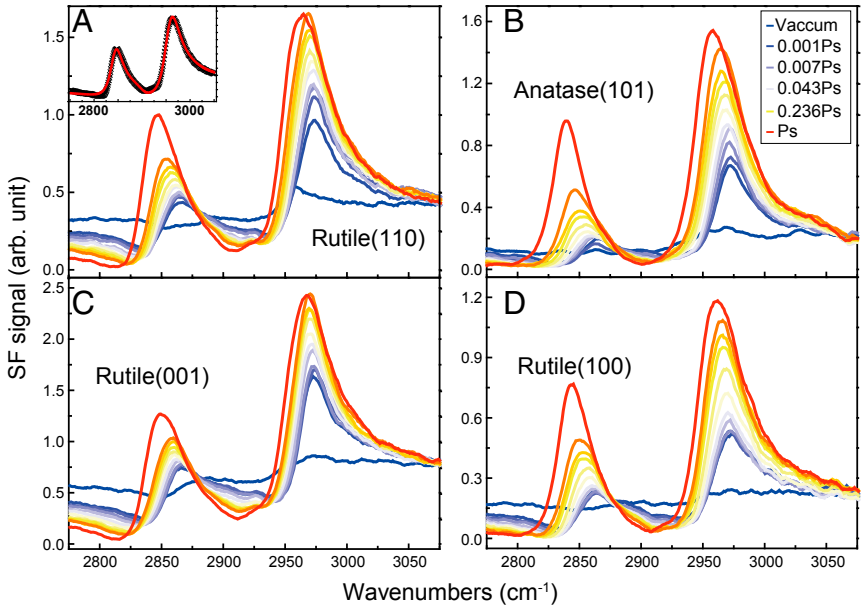

Fig. 1. SFVS of methanol adsorbed on various TiO_2 single-crystal surfaces: (*A*) rutile(110), (*B*) anatase(101), (*C*) rutile(001), and (*D*) rutile(100). Different colors refer to spectra taken under different methanol vapor pressures as labeled in *B*. All spectra are dominated by the FR-coupled CH_3 symmetric stretch mode and bending overtone at ~2,840–2,860 cm^{-1} and ~2,950–2,965 cm^{-1}, respectively. (*A*, *Inset*) Fit of the spectrum on rutile(110) under saturated vapor pressure (P_S). All spectra were taken with SSP (S-SF, S-NIR, P-IR) input/output polarization.

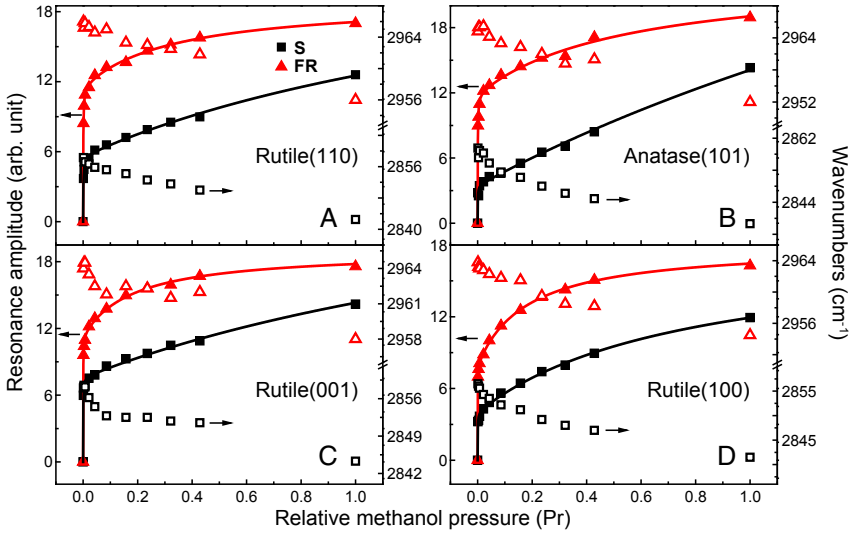

Fig. 2. Resonance amplitudes (solid symbols) and frequencies (hollow symbols), of the methanol FR-coupled CH_3 symmetric stretch mode (squares) and bending overtone (triangles) modes versus vapor pressure (relative to saturation pressure) on four TiO_2 single-crystal surfaces: (*A*) rutile(110), (*B*) anatase(101), (*C*) rutile(001), and (*D*) rutile(100). All data were extracted from fitting the spectra in Fig. 1. Solid lines are guides to eyes.

dependence would describe the adsorption isotherm (29, 30, 49). However, this is not the case as seen in Fig. 2, which shows that A_{r+} and A_{FR} vary differently with pressure. The discordance arises because A_{r+} and A_{FR} depend on the FR coupling strength (44, 50), which originates from the anharmonicity of the intramolecular potential and is sensitive to the environment of the molecule (51–54). Specifically, the FR coupling strength varies with the methanol vapor pressure and thus contributes to the dependence of A_{r+} and A_{FR} on pressure. As we shall discuss later, such effect on A_{r+} and A_{FR} can be extracted in the spectral analysis, and the procedure then allows us to extract the adsorption isotherms from the data in Fig. 2.

Configuration and energetics of molecular adsorption on a surface determine the ensuing surface chemistry. However, for methanol adsorbed on TiO_2, despite extensive studies in the past, much has remained unclear (55). For example, there is still no consensus on whether methanol adsorbs in the molecular form or dissociates spontaneously into fragments upon adsorption (8). Theoretically, cleavage of the methanol O–H bond, and attachment of the resultant methoxy moiety (CH_3–O) to the surface titanium sites (Ti_s), was found to be somewhat more favorable than molecular adsorption on rutile(110) (10, 12), but less favorable on anatase(101) (11). Experimentally, on the other hand, TPD and X-ray photoelectron spectroscopy studies concluded that methanol adsorbed in the molecular form on both rutile(110) and anatase(101) (14), and STM studies showed that methanol dissociation only occurred near the oxygen vacancy sites on rutile(110) (24). Calculation by Ferris and Wang (9) suggested that dissociative adsorption of methanol was favored on the rutile(100) surface, but TPD measurement detected methanol dissociation mostly at defect sites on rutile(100) and desorption of only methanol molecules from rutile(001) at 300 K (18, 19).

Since methanol and methoxy have distinguishable vibrational modes, SFVS can be a powerful tool to resolve this issue. The CH_3-r^+ and FR modes of methoxy at 2,828 and 2,935 cm^{-1}, respectively, were observed by Shultz and coworkers (31–34) using SFVS on thin-film samples of anatase nanoparticles comprising (101) and (001) facets at room temperature. Ren and coworkers (36, 37) also detected the same methoxy modes from rutile(110) in UHV at low temperature. In contrast, there is no trace of the presence of methoxy on all four single-crystal surfaces of TiO_2 at room temperature in our SFVS measurements (Fig. 1). UV irradiation supposedly can create holes and/or surface oxygen vacancies on TiO_2 to help cleave methanol molecules (4, 5, 8), but we still could not detect any methoxy in our spectra except for an enhanced nonresonant background (43). Apparently, methanol dissociation is either unfavorable or unstable on these single-crystal surfaces under room temperature and ambient pressure. Previous studies proposed that the back-conversion energy barrier for dissociation of water and methanol is small (16), such that dissociated fragments may not last long before they recombine, or react with other surface species and desorb. This scenario can explain why methanol dissociation appeared at low temperature and under low methanol vapor pressure (24, 37). At room temperature and elevated methanol pressure, the short-lived methoxy, if present, could only be captured by time-resolved SFVS. We note, however, that we actually could observe the appearance of strong methoxy modes as soon as the laser pulses inflicted damages (56) on the TiO_2 surfaces (Fig. 3*A*). This is in accordance with the strong showing of methoxy signals on nanoparticles (33, 34), suggesting that defects such as step edges and boundaries between facets, and/or the anatase (001) facets perhaps being more active, may serve as the active sites for methanol dissociation and stabilization of dissociated fragments (33, 34). Further investigation is needed to pinpoint and identify the functional defect structure for methanol dissociation.

Average orientation of adsorbed methanol molecules on TiO_2 can be determined from the polarization dependence of the CH_3-r^+ mode (29). In all cases, the measured ratios of the PPP and SSP mode amplitudes were nearly the same. Assuming the C_3 axis of methyl group is tilted on average by an angle θ_M from the surface normal, we found $\theta_M \sim 40$–$50°$, similar to that obtained by Ren and coworkers (35) (*SI Appendix*, Figs. S2 and S3). Compared with adsorption on fused silica, methanol molecules tilt more toward the TiO_2 surfaces.

As mentioned earlier, the amplitudes of the r^+ and FR modes, A_{r+} and A_{FR}, depend appreciably on FR coupling. If the effect can be separated from A_{r+} and A_{FR}, the resultant A^0_{r+} and $A^0_{2\delta}$ should be directly proportional to the surface density of methanol, and its variation with methanol vapor pressure will yield the proper adsorption isotherm. Note, however, the original amplitude of $A^0_{2\delta}$ should be very weak without FR coupling. To disengage the FR coupling effect and find A^0_{r+} and $A^0_{2\delta}$, we use the

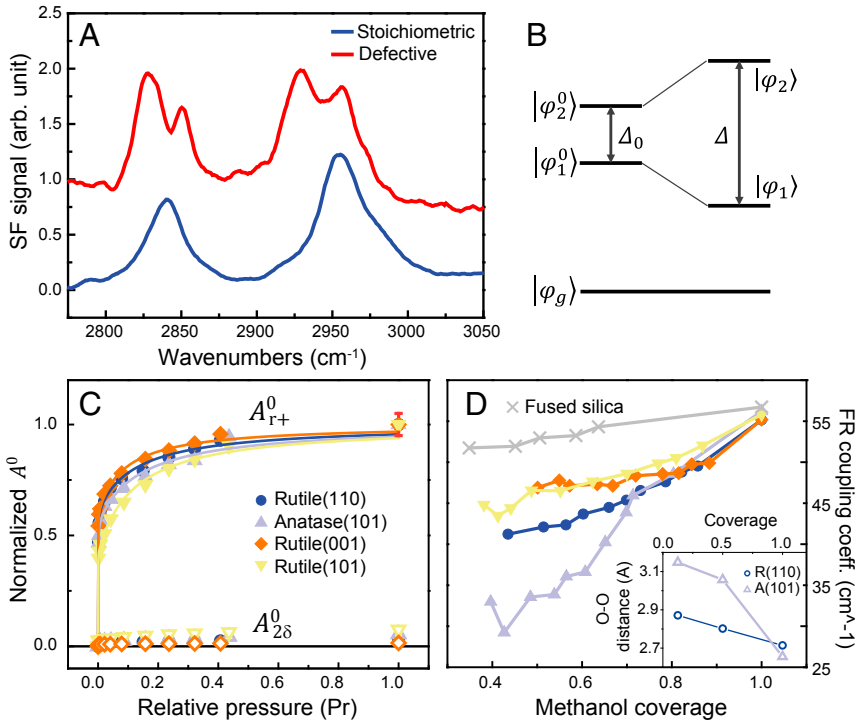

Fig. 3. Adsorption configuration and Fermi resonance effect. (*A*) SF spectra from stoichiometric (blue) and defective (red) anatase(101) surfaces in saturated methanol vapor. Curves are vertically displaced for clarity. Two extra peaks from the defective surface are attributed to methoxy. (*B*) Energy-level diagrams depicting further separation of two vibrational excitation levels by FR coupling. $|\varphi_i^0\rangle$ and $|\varphi_i\rangle$ $(i = 1, 2)$ denote the uncoupled and coupled excited states, respectively, and $|\varphi_g\rangle$ refers to the ground state. (*C*) Amplitudes of uncoupled methanol CH_3 symmetric stretch mode (A^0_{r+}, solid symbols) and bending overtone mode ($A^0_{2\delta}$, hollow symbols) versus methanol pressure deduced from the SF spectra for different TiO_2 crystal surfaces. Solid curves are fits using the two-site Langmuir adsorption model. (*D*) Deduced FR coupling coefficients of adsorbed methanol on the four TiO_2 crystal surfaces versus methanol coverage with the same color label as in *C*. The case of methanol on fused silica (gray crosses) is shown for comparison. (*D*, *Inset*) Calculated average O–O distance of H bonds formed by methanol molecules on rutile(110) and anatase(101) at different coverages.

well-established two-level model with anharmonic coupling, which was applied to methanol in the liquid phase (50, 51). Fermi resonance arises from intramolecular coupling, but is expected to be perturbed by molecules' interactions with neighboring molecules or the environment (52, 53). The model applied to liquid methanol should also be applicable to methanol adsorbed on surfaces. Let the uncoupled states be $|\varphi^0_{r+}\rangle$ and $|\varphi^0_{2\delta}\rangle$, and the coupled states be $|\varphi_{r+}\rangle$ and $|\varphi_{FR}\rangle$ (Fig. 3*B*), and the energy separation between the two uncoupled (coupled) states be $\Delta_0(\Delta)$. The uncoupled and coupled states must be related by

$$\begin{aligned}|\varphi^0_{r+}\rangle &= s|\varphi_{r+}\rangle + t|\varphi_{FR}\rangle\\ |\varphi^0_{2\delta}\rangle &= t|\varphi_{r+}\rangle - s|\varphi_{FR}\rangle\\ \text{and } s &= \sqrt{\frac{\Delta+\Delta_0}{2\Delta}},\ t = \sqrt{\frac{\Delta-\Delta_0}{2\Delta}}.\end{aligned} \quad [2]$$

The ratio of the spectral intensities for the vibrational transitions from the ground state to the two uncoupled (coupled) states is $I^0_{r+}/I^0_{2\delta}$ (I_{r+}/I_{FR}), with

$$\frac{I_{r+}}{I_{FR}} = R = \left(\frac{\sqrt{\Delta+\Delta_0}\ \sqrt{R_0}-\sqrt{\Delta-\Delta_0}}{\sqrt{\Delta-\Delta_0}\ \sqrt{R_0}+\sqrt{\Delta+\Delta_0}}\right)^2,\ \frac{I^0_{r+}}{I^0_{2\delta}} = R_0,$$

where $I^0_{2\delta} \approx 0$ without FR coupling and $R \approx \Delta + \Delta_0/\Delta - \Delta_0$ (50). Now that Δ and R are both available from the measured vibrational spectra, Δ_0 and hence s and t can all be deduced. The FR coupling coefficient W is related to Δ and Δ_0 by

$$\Delta^2 = \Delta_0^2 + 4W^2.$$

Following Eq. **2** and knowing $A_i \propto \langle\varphi_i|\hat{H}_{\text{int}}|\varphi_g\rangle$, we find

$$A^0_{r+} = sA_{r+} + tA_{FR},\ A^0_{2\delta} = tA_{r+} - sA_{FR}.$$

From the experimentally deduced R, Δ, A_{r+}, and A_{FR}, we can then calculate A^0_{r+} and $A^0_{2\delta}$, which are plotted in Fig. 3*C* as functions of p_r for the four TiO_2 surfaces. As expected, $A^0_{2\delta}$ is negligible in all cases, showing the self-consistency of the derivation. Since the methanol orientation remains unchanged with pressure, the dependence of A^0_{r+} on p_r effectively describes the adsorption isotherm. The deduced FR coupling coefficients W are plotted in Fig. 3*D* as functions of methanol coverage, with the normalized maximum A^0_{r+} in Fig. 3*C* taken as the full coverage ($\vartheta = 1$).

The Langmuir model is known to be a good approximation to describe adsorption of short-chain alcohols on oxide surfaces (34, 49). Here the data points for methanol adsorption on the four surfaces of TiO_2 in Fig. 3*C* can all be well fitted by the Langmuir adsorption isotherm with two adsorption sites (49) (solid curves in Fig. 3*C*),

$$\vartheta = \frac{N}{N_{\max}} = \frac{ap_r}{e^{\Delta G^0_a/RT}+p_r} + \frac{bp_r}{e^{\Delta G^0_b/RT}+p_r},$$

$$a + b = 1,$$

where a and b refer to the fraction of two different types of adsorption sites, and ΔG^0_a and ΔG^0_b are the corresponding Gibbs

free energies of adsorption. The deduced values of a, ΔG_a^0, and ΔG_b^0 are listed in Table 1. Within experimental uncertainty, they are quite similar for the four different TiO_2 surfaces: a ranges from ~42 to 62%, $\Delta G_a^0 \approx -20 \pm 3$ kJ/mol, and $\Delta G_b^0 \approx -5 \pm 1$ kJ/mol. Stronger adsorption on the a site up to about a half coverage is responsible for the initial rise of the isotherms. According to ab initio calculations on both rutile (110) and anatase(101) (refs. 10 and 11 as well as ours in *SI Appendix*, section 3), the most stable adsorption configuration for methanol is with the methanol oxygen (O_m) facing the low-coordinated titanium sites (Ti_s) on the surface. The heat of adsorption, $\Delta H_{Ti}^0 = \Delta G_{Ti}^0 + T\Delta S$, is in the range of ~−60 to −70 kJ/mol at about half coverage (10, 11) (*SI Appendix*, Table S1). Following the approach by Shultz and coworkers (34), we estimated the entropy change to be $\Delta S_{tran} \approx -0.15$ kJ/(mol·K) for translational degrees of freedom, and $\Delta S_{rot} \approx -0.08$ kJ/(mol·K) for rotational degrees of freedom (*SI Appendix*, section 4). At room temperature, we expect the adsorbed methanol to lose translational degrees of freedom, but can keep rotational degrees of freedom around the adsorption site. We then found $\Delta H_{Ti}^0 - T\Delta S_{tran} \approx -15$ to −25 kJ/mol at 300 K, close to the value of ΔG_a^0 given above. This agreement indicates that methanol adsorbed at the a site should have the configuration with its O_m attached to Ti_s.

At high methanol coverage, different adsorption configurations have been proposed theoretically (10, 11, 13, 36). Since for site b, $\Delta G_b^0 \approx -5$ kJ/mol is typical for adsorption of short-chain alcohols on oxides through hydrogen bonding at 300 K (57), it suggests that above half coverage, methanol begins to adsorb with its hydrogen attached to a bridging oxygen (O_s) on TiO_2 via H bonding and/or its oxygen accepting a H bond from a neighboring methanol molecule. This is more in agreement with the predicted configuration of ref. 11 for anatase(101); our ab initio calculation on anatase(101) and rutile(110) came up with a similar configuration (Fig. 4*D*). We therefore associate methanol adsorption at the b site to such a H-bonding configuration. The cartoons in Fig. 4 summarize the results of our ab initio calculations on methanol adsorption on anatase(101) and rutile(110) that support the picture described above. Methanol adsorbs predominantly in the molecular form. At low vapor pressure, the coverage increases rapidly with pressure and methanol adsorbs with its oxygen (O_m) attached to Ti_s on the surface of TiO_2 until the coverage reaches about half coverage (Fig. 4 *A* and *C*). Afterward, the coverage grows more slowly with pressure, and methanol now adsorbs by forming H bonds with O_s of TiO_2, and H of a neighboring methanol molecule adsorbed at Ti_s (Fig. 4 *B* and *D*). It is noted that molecules adsorbed to Ti_s and O_s do not form a flat monolayer but are arranged in a "bilayer-like" structure (11), so they are sometime denoted as the first and second monolayers, respectively.

The above results show that in terms of the Gibbs free energy, there is not much difference for methanol adsorption on the four TiO_2 surfaces. Our ΔG_a^0 is also not very different from ΔG^0 of ~−20 kJ/mol found for methoxy adsorption on nanocrystalline TiO_2 surfaces (32, 34). In fact, this seems to be common for short-chain alcohol adsorbed on oxides [ΔG^0 ~ −19 kJ/mol for methanol on fused silica (*SI Appendix*, Fig. S4), and ΔG^0 ~ −16 kJ/mol for ethanol on fused silica (49)]. More sensitive indicators are needed to differentiate methanol adsorption on different surface structures. The FR coupling can serve as such an indicator, as it is known to be sensitive to the molecular environment (50–54). As seen in Fig. 3*D*, the FR coupling coefficient W is very different for methanol adsorbed on different TiO_2 surfaces, and also shows strong dependence on the methanol coverage. We also plot W of methanol adsorbed on a fused silica surface in Fig. 3*D* for comparison, which clearly has a much weaker coverage dependence than on TiO_2 surfaces. At the full surface coverage, W converges to about 55 cm^{-1} for adsorbed methanol on all surfaces. The value is close to that of methanol in the liquid phase (~53 cm^{-1}) (50), indicating that methanol senses more a liquid-like environment when the surface coverage is high. In this case, as in the case of liquid, all adsorbed methanol molecules have both their oxygen and hydrogen of OH moieties H-bonded.

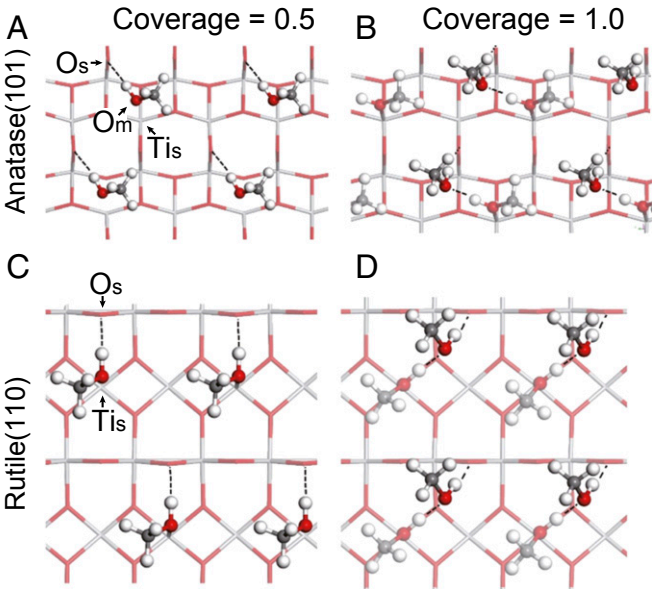

Fig. 4. Calculated adsorption configurations (top view) of methanol on (*A*) anatase(101), half coverage; (*B*) anatase(101), full coverage; (*C*) rutile(110), half coverage; and (*D*) rutile(110), full coverage. TiO_2 lattices are described by the skeletal model (Ti in gray and O in red), and methanol molecules by the ball-and-stick model (C in dark gray, O in red, and H in white). Low-coordinated surface titanium (Ti_s), surface oxygen (O_s) sites, and oxygen on methanol are indicated by arrows. Dashed lines represent hydrogen bonds.

Table 1. Experimentally deduced fraction of adsorption site *a*, and Gibbs free energies for adsorption sites *a* and *b*, on four different TiO_2 single-crystal surfaces

Surface	a	ΔG_a^0, kJ/mol	ΔG_b^0, kJ/mol
Rutile(110)	0.62 ± 0.02	−18.9 ± 0.6	−5.0 ± 0.4
Anatase(101)	0.56 ± 0.03	−19.5 ± 1.2	−4.8 ± 0.5
Rutile(001)	0.61 ± 0.02	−21.1 ± 1.0	−5.9 ± 0.3
Rutile(100)	0.42 ± 0.03	−22.5 ± 3.5	−5.3 ± 0.3

At low surface coverage, however, methanol molecules mainly adsorb to Ti_s with their O_m. The hydrogen on methanol OH bond (H_m) can still form H bond with O_s of TiO_2, but it is weak because of the large separation. This decrease of the H-bonding strength can accordingly reduce the FR coupling (52). To see that the decrease of W correlates with the reduction of H-bonding strength on methanol molecules, we calculated the average O–O distance of H bonds formed by methanol molecules on anatase(101) and rutile(110), shown in the Fig. 3*D* (*Inset*). At full coverage, the bond lengths are nearly the same for the two surfaces, but at low coverage the H bonds on anatase(101) are appreciably longer than on rutile(110), indicating a much weaker H-bonding strength (58) and hence a lower W. As the breakage of methanol OH bond and the attachment of H_m to O_s initiates the dissociation of methanol (16, 17), the hydrogen-bonding strength can appreciably affect surface reactions of methanol on TiO_2. Indeed, the recent study by Yang et al. (41) has revealed a profound effect of hydrogen bonds on water dissociation on TiO_2, that while individual H bonds

promote dissociation, an extended H-bonding network inhibits the reaction. Hence the different bonding strength between methanol H_m and O_s is likely to contribute to the different reactivity observed for rutile and anatase. The result here also shows that compared with the Gibbs free energy, the FR coupling can reveal more information on interaction between adsorbates and substrates. More details on how FR coupling relates to molecular adsorption on a surface await further investigation.

Conclusions

We have used SF vibrational spectroscopy to study methanol adsorption on four crystalline surfaces of TiO_2 at room temperature and under methanol vapor pressure ranging from 0.1 to 100% saturation value. The experimental results are complemented by ab initio calculations. In all cases, methanol appeared to adsorb on TiO_2 in the molecular form, but dissociate into methoxy on highly defective surfaces. The SF vibrational spectra allow deduction of the FR coupling coefficient for adsorbed methanol in different environments as well as the adsorption isotherm for different TiO_2 surfaces. For all four TiO_2 surfaces, the adsorption isotherm could be fit by a Langmuir model of two adsorption sites with adsorption free energies of ∼−20 kJ/mol and ∼−5 kJ/mol, respectively, indicating that the adsorption energetics are very similar on the four TiO_2 surfaces. However, the FR coupling coefficient for methanol adsorbed on the four surfaces is significantly different for different surfaces, and can serve as a better sensor to gauge how methanol interact with different surface structures.

Materials and Methods

Sample Preparation. Rutile(110), (100), and anatase(101) crystals of 2-mm thickness and rutile(001) crystal of 5-mm thickness, purchased from SurfaceNet and MaTeck, respectively, were cleaned by successively sonicating in acetone (analytically pure; Shanghai Dahe Chemicals Co. Ltd), ethanol (analytically pure; Shanghai Zhengxing No. 1 Chemical Plant), and deionized water (18.2 MΩ·cm) each for 30 min. The samples were then placed in the measurement chamber purged with pure oxygen, followed by UV-ozone treatment for 10 min to remove organic contamination (monitored by sum-frequency vibration spectroscopy), and sit in pure oxygen to heal surface oxygen vacancies before the chamber was evacuated for dosing methanol. Adsorbed OH species are known to be difficult to remove, but should be at a low coverage as there was no prominent OH resonant signal at above 3,000 cm^{-1} (33). The chamber has a base pressure <5 Pa. A BaF_2 window coated by 35-nm-thick SiO_2 film was used to transmit input and outgoing beams, and was placed at ∼3–4 mm above the sample to reduce the absorption of IR light by the methanol vapor. The vapor pressure of methanol (99.9%; J&K Scientific) in the chamber was controlled by a microadjustable valve, and measured by a Pirani vacuum gauge.

SFG Measurements. The broadband, multiplex scheme of SFVS was used in our measurements. A regenerative amplifier (Spitfire; Spectra Physics) seeded by a Ti:sapphire oscillator (MaiTai SP; Spectra Physics) produced ∼4 W of 800-nm, 35-fs pulses at 1-kHz repetition rate. About 2.6 W of the beam was used to generate a narrowband beam of ∼0.4-nm bandwidth by passing through a Bragg filter (BPF-800; OptiGrate), and the rest was used to pump an optical parametric amplifier (TOPAS-C; Spectra Physics) and generate a broadband IR beam (FWHM ∼ 500 cm^{-1}) centered at about 2,900 cm^{-1} by pumping an optical parametric amplifier (TOPAS-C; Spectra Physics) followed by a difference frequency generation stage (59). The 800-nm narrowband pulse and the broadband IR pulse with pulse energy of about 15 and 8 μJ, respectively, were focused and overlapped onto a spot of ∼0.5 mm on the sample surface with incident angles of 45° and 57°, respectively. The generated SFG signal was detected by a spectrograph (Acton SP300i; Princeton Instrument) and CCD camera (PyLoN:400BR eXcelon; Princeton Instruments). The observed spectra were normalized to that from a *z*-cut α-quartz. The quartz reference without methanol vapor and with saturated methanol vapor pressure showed negligible intensity difference. All experiments were conducted at room temperature.

Ab Initio Calculation. Calculations were carried out using the spin-polarized density-functional theory with the generalized gradient approximation of Perdew–Burke–Ernzerhof implemented in the VASP code. Both anatase(101) and rutile(110) surfaces were modeled by a (4 × 2) surface supercell. The *K*-point sampling was restricted to the gamma point due to the large supercell size. The interaction between core and valence electrons was described by the projector-augmented wave method with an energy cutoff of 400 eV. The force convergence criterion was 0.05 eV/Å (60–63).

ACKNOWLEDGMENTS. The research is funded by the National Natural Science Foundation of China and the National Basic Research Program of China under Grant Agreements 2016YFA0300900, 2014CB921600, 11622429, 11574340, 11374065, and 11290161. Y.R.S. acknowledges support from the Director, Office of Science, Office of Basic Energy Sciences, Materials Sciences and Engineering Division, of the US Department of Energy under Contract DE-AC03-76SF00098.

1. Yang HG, et al. (2008) Anatase TiO_2 single crystals with a large percentage of reactive facets. *Nature* 453:638–641.
2. Tachikawa T, Yamashita S, Majima T (2011) Evidence for crystal-face-dependent TiO_2 photocatalysis from single-molecule imaging and kinetic analysis. *J Am Chem Soc* 133: 7197–7204.
3. Yu J, Low J, Xiao W, Zhou P, Jaroniec M (2014) Enhanced photocatalytic CO_2-reduction activity of anatase TiO_2 by coexposed 001 and 101 facets. *J Am Chem Soc* 136: 8839–8842.
4. Diebold U (2003) The surface science of titanium dioxide. *Surf Sci Rep* 48:53–229.
5. Fujishima A, Zhang X, Tryk D (2008) TiO_2 photocatalysis and related surface phenomena. *Surf Sci Rep* 63:515–582.
6. Henderson MA (2011) A surface science perspective on TiO_2 photocatalysis. *Surf Sci Rep* 66:185–297.
7. Schneider J, et al. (2014) Understanding TiO_2 photocatalysis: Mechanisms and materials. *Chem Rev* 114:9919–9986.
8. Thomas AG, Syres KL (2012) Adsorption of organic molecules on rutile TiO_2 and anatase TiO_2 single crystal surfaces. *Chem Soc Rev* 41:4207–4217.
9. Ferris KF, Wang L (1998) Electronic structure calculations of small molecule adsorbates on (110) and (100) TiO_2. *J Vac Sci Technol A* 16:956–960.
10. Bates SP, Gillan MJ, Kresse G (1998) Adsorption of methanol on TiO_2(110): A first-principles investigation. *J Phys Chem B* 102:2017–2026.
11. Tilocca A, Selloni A (2004) Methanol adsorption and reactivity on clean and hydroxylated anatase(101) surfaces. *J Phys Chem B* 108:19314–19319.
12. de Armas RS, Oviedo J, San Miguel MA, Sanz JF (2007) Methanol adsorption and dissociation on t TiO_2(110) from first principles calculations. *J Phys Chem C* 111: 10023–10028.
13. Zhao J, Yang J, Petek H (2009) Theoretical study of the molecular and electronic structure of methanol on a TiO_2(110) surface. *Phys Rev B* 80:235411–235416.
14. Herman GS, Dohnálek Z, Ruzycki N, Diebold U (2003) Experimental investigation of the interaction of water and methanol with anatase-TiO_2(101). *J Phys Chem B* 107: 2788–2795.
15. Xu C, et al. (2013) Strong photon energy dependence of the photocatalytic dissociation rate of methanol on TiO_2(110). *J Am Chem Soc* 135:19039–19045, and erratum (2014) 136:4794.
16. Guo Q, et al. (2012) Stepwise photocatalytic dissociation of methanol and water on TiO_2(110). *J Am Chem Soc* 134:13366–13373.
17. Xu C, et al. (2014) Molecular hydrogen formation from photocatalysis of methanol on anatase-TiO_2(101). *J Am Chem Soc* 136:602–605.
18. Kim KS, Barteau MA (1989) Reactions of methanol on TiO_2(001) single crystal surfaces. *Surf Sci* 223:13–32.
19. Roman E, Bustillo FJ, de Segovia JL (1990) Adsorption of methanol on the low Ti^{+3} point defects of the TiO_2(001) surface at 300 K. *Vacuum* 41:40–42.
20. Setvín M, et al. (2013) Reaction of O_2 with subsurface oxygen vacancies on TiO_2 anatase (101). *Science* 341:988–991.
21. Setvin M, et al. (2014) Direct view at excess electrons in TiO_2 rutile and anatase. *Phys Rev Lett* 113:086402.
22. Wang Y, et al. (2013) Role of point defects on the reactivity of reconstructed anatase titanium dioxide (001) surface. *Nat Commun* 4:2214.
23. Schaub R, et al. (2001) Oxygen vacancies as active sites for water dissociation on rutile TiO_2(110). *Phys Rev Lett* 87:266104.
24. Zhou C, et al. (2010) Site-specific photocatalytic splitting of methanol on TiO_2(110). *Chem Sci* 1:575–580.
25. Shen YR (2011) Surface nonlinear optics [Invited]. *J Opt Soc Am B* 28:A56–A66.
26. Somorjai GA, Beaumont SK, Alayoglu S (2011) Determination of molecular surface structure, composition, and dynamics under reaction conditions at high pressures and at the solid-liquid interface. *Angew Chem Int Ed Engl* 50:10116–10129.
27. Beaman DK, Robertson EJ, Richmond GL (2012) Ordered polyelectrolyte assembly at the oil-water interface. *Proc Natl Acad Sci USA* 109:3226–3231.
28. Liu W, Zhang L, Shen YR (2005) Interfacial layer structure at alcohol/silica interfaces probed by sum-frequency vibrational spectroscopy. *Chem Phys Lett* 412:206–209.
29. Liu WT, Zhang L, Shen YR (2006) Interfacial structures of methanol:water mixtures at a hydrophobic interface probed by sum-frequency vibrational spectroscopy. *J Chem Phys* 125:144711.

30. Zhang L, Liu W, Shen YR, Cahill DG (2007) Competitive molecular adsorption at liquid/solid interfaces: A study by sum-frequency vibrational spectroscopy. *J Phys Chem C* 111:2069–2076.
31. Wang C, Groenzin H, Shultz MJ (2003) Molecular species on nanoparticulate anatase TiO_2 film detected by sum frequency generation: Trace hydrocarbons and hydroxyl groups. *Langmuir* 19:7330–7334.
32. Wang C, Groenzin H, Shultz MJ (2004) Surface characterization of nanoscale TiO_2 film by sum frequency generation using methanol as a molecular probe. *J Phys Chem B* 108:265–272.
33. Wang CY, Groenzin H, Shultz MJ (2004) Direct observation of competitive adsorption between methanol and water on TiO_2: An in situ sum-frequency generation study. *J Am Chem Soc* 126:8094–8095.
34. Wang CY, Groenzin H, Shultz MJ (2005) Comparative study of acetic acid, methanol, and water adsorbed on anatase TiO_2 probed by sum frequency generation spectroscopy. *J Am Chem Soc* 127:9736–9744.
35. Liu A, Liu S, Zhang R, Ren Z (2015) Spectral identification of methanol on TiO_2(110) surfaces with sum frequency generation in the C-H stretching region. *J Phys Chem C* 119:23486–23494.
36. Liu S, et al. (2015) Coverage dependence of methanol dissociation on TiO_2(110). *J Phys Chem Lett* 6:3327–3334.
37. Feng R, et al. (2015) In situ studies on the dissociation and photocatalytic reactions of CH_3OH on TiO_2 thin film by sum frequency generation vibrational spectroscopy. *J Phys Chem C* 119:9798–9804.
38. Feng R, et al. (2015) Methanol adsorption on TiO_2 film studied by sum frequency generation vibrational spectroscopy. *Chin J Chem Phys* 28:11–16.
39. Kataoka S, et al. (2004) Investigation of water structure at the TiO_2/aqueous interface. *Langmuir* 20:1662–1666.
40. Jang JH, Lydiatt F, Lindsay R, Baldelli S (2013) Quantitative orientation analysis by sum frequency generation in the presence of near-resonant background signal: Acetonitrile on rutile TiO_2 (110). *J Phys Chem A* 117:6288–6302.
41. Yang W, et al. (2016) Effect of the hydrogen bond in photoinduced water dissociation: A double-edged sword. *J Phys Chem Lett* 7:603–608.
42. Liu WT, Shen YR (2014) In situ sum-frequency vibrational spectroscopy of electrochemical interfaces with surface plasmon resonance. *Proc Natl Acad Sci USA* 111:1293–1297.
43. Cao Y, et al. (2016) Evolution of anatase surface active sites probed by in situ sum-frequency phonon spectroscopy. *Sci Adv* 2:e1601162.
44. Ishiyama T, Sokolov VV, Morita A (2011) Molecular dynamics simulation of liquid methanol. I. Molecular modeling including C-H vibration and Fermi resonance. *J Chem Phys* 134:024509.
45. Yu Y, et al. (2013) Complete Raman spectral assignment of methanol in the C-H stretching region. *J Phys Chem A* 117:4377–4384.
46. Stanners CD, et al. (1995) Polar ordering at the liquid-vapor interface of n-alcohols (C_1-C_8). *Chem Phys Lett* 232:407–413.
47. Ma G, Allen HC (2003) Surface studies of aqueous methanol solutions by vibrational broad bandwidth sum frequency generation spectroscopy. *J Phys Chem B* 107:6343–6349.
48. Chen H, Gan W, Lu R, Guo Y, Wang HF (2005) Determination of structure and energetics for Gibbs surface adsorption layers of binary liquid mixture 2. Methanol + water. *J Phys Chem B* 109:8064–8075.
49. Xu H, Zhang D, Hu J, Tian C, Shen YR (2015) Structure of the submonolayer of ethanol adsorption on a vapor/fused silica interface studied with sum frequency vibrational spectroscopy. *J Phys Chem A* 119:4573–4580.
50. Devendorf GS, Hu MA, Ben-Amotz D (1998) Pressure dependent vibrational Fermi resonance in liquid CH_3OH and CH_2Cl_2. *J Phys Chem A* 102:10614–10619.
51. Schwartz M, Moradi-Araghi A, Koehler WH (1980) Fermi resonance in aqueous methanol. *J Mol Struct* 63:279–285.
52. Greve C, Nibbering ETJ, Fidder H (2013) Hydrogen-bonding-induced enhancement of Fermi resonances: A linear IR and nonlinear 2D-IR study of aniline-d_5. *J Phys Chem B* 117:15843–15855.
53. Tian K, Zhang B, Ye S, Luo Y (2015) Intermolecular interactions at the interface quantified by surface-sensitive second-order Fermi resonant signals. *J Phys Chem C* 119:16587–16595.
54. Schwartz M, Moradi-Araghi A, Koehler WH (1982) Solvent and temperature dependence of the Fermi resonance parameters in methanol. *J Mol Struct* 81:245–252.
55. Pan J, Liu G, Lu GQ, Cheng HM (2011) On the true photoreactivity order of 001, 010, and 101 facets of anatase TiO2 crystals. *Angew Chem Int Ed Engl* 50:2133–2137.
56. Furusawa K, et al. (2000) Femtosecond laser micromachining of TiO_2 crystal surface for robust optical catalyst. *J Appl Phys* 87:1604–1609.
57. Sedov IA, Solomonov BN (2012) Gibbs free energy of hydrogen bonding of aliphatic alcohols with liquid water at 298 K. *Fluid Phase Equilib* 315:16–20.
58. Jeffrey GA (1997) *An Introduction to Hydrogen Bonding* (Oxford Univ Press, Oxford).
59. Cao Y, Liu X, Liu W (2017) A broadband and compact femtosecond delay compensator with birefringent crystals. *Laser Phys Lett* 14:035302.
60. Kresse G, Hafner J (1993) Ab initio molecular dynamics for liquid metals. *Phys Rev B Condens Matter* 47:558–561.
61. Perdew JP, Wang Y (1992) Accurate and simple analytic representation of the electron-gas correlation energy. *Phys Rev B Condens Matter* 45:13244–13249.
62. Blöchl PE, Jepsen O, Andersen OK (1994) Improved tetrahedron method for Brillouin-zone integrations. *Phys Rev B Condens Matter* 49:16223–16233.
63. Kresse G, Joubert D (1999) From ultrasoft pseudopotentials to the projector augmented-wave method. *Phys Rev B* 59:1758–1775.